Experimental Assessment of the Coarray Concept for DoA Estimation in Wireless Communications

Jiachen Wang, *Student Member, IEEE*, Hantao Xu, *Student Member, IEEE*, Geert J. T. Leus, *Fellow, IEEE*, and Guy A. E. Vandenbosch, *Fellow, IEEE*

***Abstract*— The direction of arrival (DoA) estimation performance of three different coarray structures, namely, the nested array, the coprime sampling array, and the sparse ruler array are presented and compared. The coarray concept makes it possible to detect the DoAs of much more sources than the number of physical antennas. Crucial is that for the first time, these coarrays are investigated based on real measurements conducted on a demonstrator platform. Based on the results obtained, the conclusion is clear. The MUSIC algorithm-based coarray concept with spatial smoothing is not suitable for DoA estimation in practical circumstances due to the unavoidable multipath phenomenon.**

***Index Terms*— Coarray, coprime sampling array (CA), data measurements, direction of arrival (DoA) estimation, MUSIC, nested array (NA), sparse ruler array (SRA), spatial smoothing.**

I. Introduction

In THE past decade, abundant research has been conducted on direction of arrival (DoA) estimation which can be applied in wireless communications, radar systems, and sonar signal processing. A key question is: how many sources can be detected by an antenna array with a fixed number of elements [1]–[3]. In 1980s, the MUSIC algorithm was conceived [4]. This algorithm calculates the autocorrelations of the signals received from the antenna elements and uses them to form a covariance matrix of the impinging signals. By applying an eigenvalue decomposition and a parameter estimation to the covariance matrix, subspace-based direction finding algorithms can reach so-called super resolution, i.e., Rayleigh resolution, compared to simple beam scanning techniques.

A key characteristic of first generation DoA algorithms is that the maximum number of detectable sources N is limited by the number of antenna elements L used in the array, i.e., $N = L - 1$. Furthermore, these algorithms suffer from coherently impinging signals, such as multipath signals originating from reflections in rooms or buildings. A spatial smoothing technique can be applied to remove the coherency of these signals and again enhance the reliability and robustness of the algorithms [5], [6]. In [7] and [8], a so-called universal steering vector is proposed and verified, both with simulations and experiments, for MUSIC-based DoA estimations, taking into account the effect of mutual coupling in the arbitrary receiving array.

In [9], the role of coarrays in aperture synthesis is considered. Methods for incoherent aperture synthesis (including correlation beamforming, intensity image addition, and incoherent aperture synthesis using subarrays) and methods for coherent aperture synthesis (including direct synthesis, complex amplitude image addition, and incoherent aperture synthesis using subarrays) are discussed in detail and compared. Based on these ideas, methods using the coarray concept are developed.

In [10], a new coarray weight synthesis method for circular and elliptical boundary arrays based on image addition is proposed. This method can be applied to both passive and active sensing. The idea of finding more sources than the number of antenna elements was tackled by using the concept of minimal redundancy arrays [11], creating an augmented covariance matrix [2], [3]. However, this technique requires the sources to be nonGaussian, as pointed out in [12].

In recent years, new concepts were adopted based on compressive sensing. A general review of compressive sensing in electromagnetics, including DoA estimation was done in [13] and [14]. In [15] and [16], compressive sensing-based algorithms work with a random subset of elements from a full uniform linear array (ULA). With several snapshots over time, this dynamic technique is able to achieve so-called "compressive sensing recovery," regenerating the full ULA from randomly selected elements [12], [17]–[19]. In [20], a review of compressive sensing-based sparse arrays is conducted.

The algorithm studied in this paper, namely, the difference coarray (DCA) algorithm targets passive sensing, and can be applied to the nested array (NA) [12], the coprime sampling array (CA) [19], and the sparse ruler array (SRA) [18]. This algorithm no longer requires the system to physically have a full ULA or any displacement of the antenna elements. Hence, many antenna elements can be turned OFF or even removed from the system, to save power and space. All three techniques can boost the number of targets that can be detected up to $O(L^2)$ [17]. All three arrays in theory have shown

Manuscript received November 30, 2017; revised February 23, 2018; accepted March 12, 2018. Date of publication March 26, 2018; date of current version May 31, 2018. *(Corresponding author: Jiachen Wang.)*

J. Wang, H. Xu, and Guy A. E. Vandenbosch are with the TELEMIC Division, Department of Electrical Engineering (ESAT), Katholieke Universiteit Leuven, 3001 Leuven, Belgium (e-mail: jwang@esat.kuleuven.be; hxu@esat.kuleuven.be; guy.vandenbosch@esat.kuleuven.be).

Geert J. T. Leus is with the Faculty of Electrical Engineering, Mathematics and Computer Science, Delft University of Technology, 2826 CD Delft, Netherlands (e-mail: g.j.t.leus@tudelft.nl).

Color versions of one or more of the figures in this paper are available online at http://ieeexplore.ieee.org.

Digital Object Identifier 10.1109/TAP.2018.2819824

promising detection resolutions and the capability of finding more sources. For all MUSIC-based coarrays, there is a "saturation" behavior in the high signal-to-noise ratio (SNR) region [20], which means that when there are more sources than the number of antenna elements, the DoA estimation error of such coarrays converges to a positive value instead of zero for an infinite SNR.

Recently, even methods to improve the performance of the coarray methods have been proposed. For NA, in [22], a calibration method with model errors has been proposed to reduce the DoA estimation errors. In [23], the two-level NA technique with a larger aperture and more degrees of freedom is introduced. A super NA, with less mutual coupling, is proposed in [24] and [25]. The most recent research is [26], where an improved NA with hole-free DCA and more degrees of freedom is proposed. The original CA has a lower degree of freedom and a lower accuracy due to the missing elements in the virtual coarray [27]. Nuclear norm minimization [28], multiple sources with moving coprime array for microphone applications [29], new beamforming techniques with extended coprime sensors [30], and temporal signal coherence [31] are proposed to improve the CA's performance.

The above-mentioned overview illustrates that a lot of research has been performed and is being performed within the signal processing community. However, antenna system designers, both in industry and in academia, point out that there is a real need for studies reporting on experimental results. Although DoA, beam steering, and other related functionalities have been studied for many years, now in a mainly theoretical way, it is obvious from our literature study that most of the new concepts have never been implemented and tested in a real demonstrator platform. According to industry, this is a major factor impeding the actual use of the algorithmic progress made. Such reports can be studied and assessed not only by industry but also by pure signal processing people, bringing (some of) them into closer contact with practical realizations and the corresponding restrictions and limitations.

As far as we can see, the performance of coarrays has only been partially verified in experiments using microphones in acoustic applications [32]–[34]. The specified virtual array technique for DoA estimation was experimentally verified for indoor terrestrial TV signal reception in [35] and for automotive radar in [36]. However, in the field of telecommunications with electromagnetic waves, the performance of the above-mentioned original arrays as well as the improved ones has been investigated only using computer simulations. They have never been evaluated while running on a real system.

In this paper, to our best knowledge for the first time, the three original coarrays are evaluated based on measurements performed on a real demonstrator platform. This platform was developed within the framework of a multiple users beam tracking system (MUBTS) [37].

The paper is structured as follows. Section II briefly discusses the coarray algorithms. Section III gives a brief introduction of the experimental platform and presents the performance and comparison of the coarrays' DoA estimation based on simulations and real-data measurements.

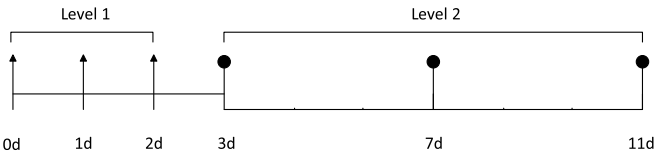

Fig. 1. Two-level NA with $P = Q = 3$ [12].

II. Coarray Algorithms

In this section, the algorithms of the NA, CA, and SRA are briefly summarized. For more details, we refer to the literature available in the signal processing community [12], [18], [19].

A. Array Signals

Suppose there are N incident waves with incident angles $\theta_1, \theta_2, \ldots, \theta_N$ and powers $\sigma_1, \sigma_2, \ldots, \sigma_N$, coming from N uncorrelated sources, exciting a non-ULA (NULA) with L elements. $\mathbf{a}(\theta)$ is the $L \times 1$ steering vector corresponding to the direction θ, whose ith element is $e^{j(2\pi/\lambda)d_i \sin(\theta)}$. d_i is the position of the ith element, which is an integer multiple of the smallest spacing in the array. A common choice of the smallest spacing is smaller or equal to half the wavelength to avoid spatial aliasing. The carrier wavelength is λ. Then, the received signal is

$$\mathbf{x}(t) = \mathbf{A}\boldsymbol{s}(t) + \mathbf{g}(t) \tag{1}$$

where $\mathbf{A} = [\mathbf{a}(\theta_1), \mathbf{a}(\theta_2), \ldots, \mathbf{a}(\theta_N)]$ is the $L \times N$ matrix of all steering vectors and $\boldsymbol{s}(t) = [s_1(t), s_2(t), \ldots, s_N(t)]^T$ is the N-dimensional vector of input signals. The spatial autocorrelation matrix is written as

$$\mathbf{R_{xx}} = E[\mathbf{x}(t)\mathbf{x}^{\boldsymbol{H}}(t)] \tag{2}$$

where $E[.]$ is the expectation operator. And it can be estimated by taking T snapshots at specific times t_i of $\boldsymbol{s}(t)$ and averaging the output over the number of snapshots [4].

B. Structuring of NULA Arrays With Three Coarrays

The coarray set of a linear array can be defined as all possible pairwise antenna separations of the original linear array [11]. Each element in the coarray set corresponds to a spatial correlation lag between an antenna pair with the same antenna separation value [18]. The coarray set provides $O(L^2)$ degrees of freedom with L physical elements, which is much larger than the original array. Hence, it enables to detect more sources than the original array. Basically, NA, CA, and SRA are the methods that yield positions of physical antenna elements in such a manner that a coarray with much larger virtual length can be synthesized from a smaller physical NULA.

1) Nested Array: A two-level NA is a combination of two ULAs: an inner ULA (level 1) with P elements and spacing $d_1 = d$ (half wavelength) and an outer ULA (level 2) with Q elements and spacing d_2. The spacing d_1 and d_2 follow the relationship $d_2 = (P + 1)d_1$. An optimal choice here is $P = Q$ [12]. In Fig. 1, an example of an NA, with in total six physical elements, is displayed. NA is possible to extend to higher levels [12].

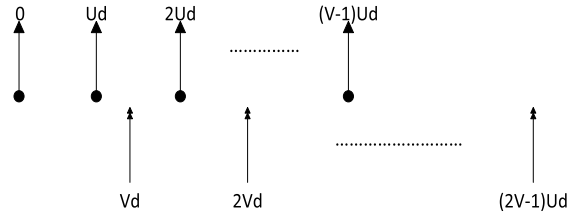

Fig. 2. Coprime pair of ULAs with spacings *Ud* and *Vd* [19].

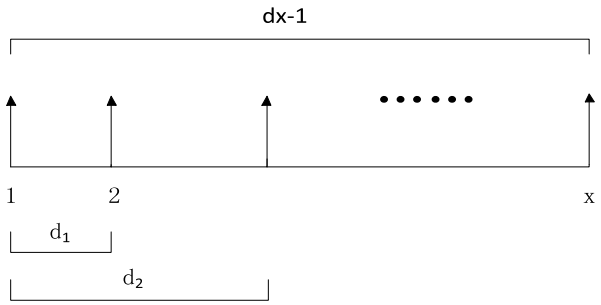

Fig. 3. Structure of an SRA [18].

An NA is able to detect up to $(P+Q)^2/4+(P+Q)/2-1$ sources.

2) Coprime Sampling Array: A CA is also a combination of two ULAs but now the two inter element spacings correspond to a pair of coprime integers, i.e., U and V times the half wavelength d. Assume that $U < V$ and that the array with Ud interspacing has $\mathrm{V}-1$ elements and that the array with Vd interspacing has $2\mathrm{U}-1$ elements(see Fig. 2). In that case, up to UV sources can be detected [19], [27].

3) Sparse Ruler Array: A ruler with X marks is considered a minimal sparse ruler if there is no ruler with $X-1$ marks that can measure up to $Y-1$ consecutive integer distances ($X < Y$), with X and Y two arbitrary integers. Placing physical array elements according to the marks of a sparse ruler with X marks, it is possible to extend such an array to a full ULA with Y elements, theoretically being able to detect $Y-1$ sources. The structure of an SRA can be seen in Fig. 3 [18]. A list of arrangements of the marks for a given length can easily be found from mathematical tables [38]. However, there is no closed form expression for designing a sparse ruler. For large Y, they are found by exhaustive search.

C. Coarray and Spatial Smoothing

The theory concerning the coarray is well elaborated in several papers (see [12], [18], [19]). For reasons of clarity, here we just summarize the basic principles. For all three arrays considered in the Section II-B, the output signal covariance matrix (2) from all the physical array elements can be written as

$$\mathbf{R_{xx}} = \mathbf{A}\mathbf{R_{ss}}\mathbf{A}^{\boldsymbol{H}} + \sigma_g^2\mathbf{I} = \mathbf{A}\begin{pmatrix}\sigma_1^2 & & & \\ & \sigma_2^2 & & \\ & & \ddots & \\ & & & \sigma_N^2\end{pmatrix}\mathbf{A}^{\boldsymbol{H}} + \sigma_g^2\mathbf{I} \tag{3}$$

where σ_n^2 is proportional to the power of each signal source, σ_g^2 is proportional to the noise power, and $\mathbf{I}$ is the identity matrix.

Vectorizing $\mathbf{R_{xx}}$ [17] delivers

$$\begin{aligned} z = \mathrm{vec}(\mathbf{R_{xx}}) &= \mathrm{vec}\left[\sum_{i=1}^{N}\sigma_i^2(\mathbf{a}(\theta_i)\mathbf{a}^{\boldsymbol{H}}(\theta_i))\right] + \sigma_g^2\mathbf{e} \\ &= \mathbf{B}(\theta_1,\theta_2,\ldots,\theta_N)\mathbf{p} + \sigma_g^2\mathbf{e} \end{aligned} \tag{4}$$

where $\mathbf{e} = \mathrm{vec}[\mathbf{I}]$, $\mathbf{p} = [\sigma_1^2,\sigma_2^2,\ldots,\sigma_N^2]^T$, and

$$\mathbf{B} = \mathbf{A}^* \odot \mathbf{A} = [\mathbf{a}(\theta_1)^* \otimes \mathbf{a}(\theta_1),\ldots,\mathbf{a}(\theta_N)^* \otimes \mathbf{a}(\theta_N)] \tag{5}$$

with $\odot$ denoting the Khatri–Rao product and $\otimes$ denoting the Kronecker product. $\mathbf{B}$ behaves like the manifold of a longer ULA, which is the coarray of the original array [12], [18], [19].

For SRA and NA, the virtual coarrays generated by the original arrays are ULAs without missing elements. The conventional spatial smoothing-based approach [12], [39], [40] can be applied to exploit the degrees of freedom of the DCA. In these two cases, all coarray lags are produced up to a maximum lag that is different for each array, and some lags appear multiple times in the vectorized data. A new matrix $\mathbf{Z_1}$ is formed from $\mathbf{Z}$ by reordering the rows in the order of increasing coarray lag, while averaging the elements of $\mathbf{Z}$ that correspond to the same lag. Spatial smoothing is applied. It is to be noted that spatial smoothing is thus not used for de-correlating uncorrelated sources in a coarray, but rather as a rank enhancing technique for the observation matrix of the coarray. Therefore, it eliminates the need to either use fourth-order cumulants or to assume quasi-stationarity of the signals. Full details can be found in [12] and [18].

Unlike SRA and NA, the coarray of CA is not uniformly linear but has missing elements. Conventional spatial smoothing is not applicable here. An extra step is necessary. This is explained as follows. For two coprime integers U and V ($U < V$), given an integer k in the range $0 \le k \le UV$, there are integers u and υ in the range $0 \le \upsilon \le V-1$ and $0 \le u \le 2U-1$ so that $k = Vu - U\upsilon$. $-k$ is produced as $k = U\upsilon - Vu$. According to this property, all differences from $-UV$ to UV can be generated, and this helps to generate $2UV+1$ degrees of freedom in a continuous range by using only $V+2U$ physical integers. Spatial smoothing can be applied to this continuous difference from $-UV$ to UV. Details can be found in [19].

For all three arrays, a new matrix $\mathbf{B_1}$ is formed with steering vectors for the virtual ULA after spatial smoothing. The spatially smoothed covariance matrix is ready to be imported into the MUSIC algorithm [12], [18], [19].

III. Measurement Setup and Results

A. Measurement Setup

In many multiple antenna systems, 3–16 antenna elements are commonly seen. Some applications require much more antennas such as radars, remote sensing systems, and imaging applications. They pose specific problems, both in the analog and the digital domain. First of all, in the digital domain, due

TABLE I
COMPARISON OF THE THREE COARRAYS REGARDING DIMENSION AND MAXIMUM NUMBER OF SOURCES WHEN SPATIAL SMOOTHING IS USED

	Dimension unit d = half wavelength			Maximum number of traceable sources		
Number of physical elements	SRA (Max.length)	NA	CA	SRA	NA	CA
4	$6d$	$5d$ (P=Q=2)	$3d$ (U=1,V=3)	6	5	3
5	$9d$	$8d$ (P=2, Q=3)	$4d$ (U=1,V=4)	9	8	4
6	$13d$	$11d$ (P=Q=3)	$9d$ (U=2,V=3)	13	11	6
7	$17d$	$15d$ (P=3, Q=4)	$6d$ (U=1,V=6)	17	15	6
8	$23d$	$19d$ (P=Q=4)	$15d$ (U=2,V=5)	23	19	10
16	$90d$	$89d$ (P=Q=8)	$63d$ (U=4,V=9)	90	89	36

to higher number of elements, a very high data processing power is required. The processing power required for L elements is in the order of $O(L^2)$ or $O(L^3)$, depending on the algorithms used [41]. Second, in the analog domain, synchronizing all antenna elements and guaranteeing that all elements behave identically to each other becomes a huge challenge. This requires specific considerations and architectures [42]. A digital-domain calibration becomes indispensable. Also, the transfer of all data from the analog to the digital subsystem is restricted by the available high-speed interfaces between the analog and the digital domain.

Therefore, considering the applicability in daily life and the current state-of-the-art in signal processing power in field-programmable gate arrays (FPGAs) and computers, we focus this research on array sizes smaller than 16 and a reasonable snapshot length of maximum 3200.

To construct a coarray synthesizable NULA, minimum four elements are needed [18]. The maximal traceable number of sources grows in a square way with the number of actual elements used. Note that the actual number depends on the fact that spatial smoothing is applied on all three coarrays [12], [17]–[19]. The number of subarrays for each method is defined as follows: (based on $D = \lambda/2$)

$$\begin{aligned} &\text{SRA}: \ \text{Length of sparse ruler} + 1 \\ &\text{NA}: \ (Q \times (P+1) - 1) + 1 \\ &\text{CA}: \ U \times V + 1. \end{aligned}$$

In Table I, a comparison is given for the three arrays regarding the maximum aperture and the maximum number of traceable sources, in terms of the number of physical elements used, starting from 4 up to 16.

From Table I, it can be seen that the sparse ruler has the largest spatial dimensions and the highest degree of freedom, i.e., the largest number of sources that can be detected, for the same number of physical elements.

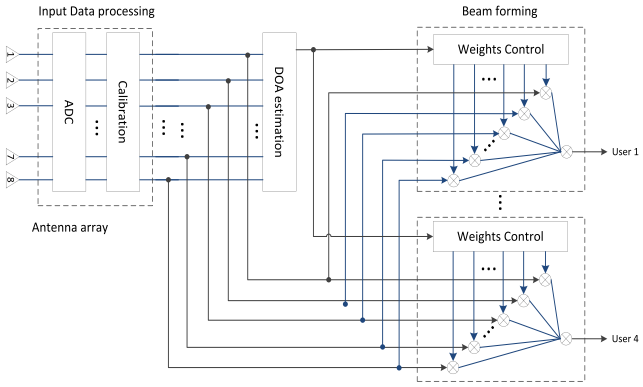

Fig. 4. Block diagram of MUBTS [37].

In [12], [18], and [19], it is clearly shown that the resolution of a DoA estimation increases with the array aperture size. The straightforward idea is then to compare these three arrays while taking the same aperture size and the same number of physical elements. However, according to Table I, it is not possible to find a perfect "match" between the three coarrays, i.e., a case where the three criteria (number of physical elements, aperture, and maximal traceable number of sources) are all the same. For the same number of actual physical antenna elements, it is clear that SRA can detect more sources than NA and much more than CA. So, in the rest of the paper, the same number of physical elements is chosen as the basis for comparison.

The algorithms discussed were implemented on the MUBTS demonstration platform. A simplified structure of this platform can be seen in Fig. 4. The DoA estimation block is used to determine the beamforming weights to separate the signals from different users. The MUBTS system supports up to 16 redistributable physical antenna elements. Full details can be found in [37]. The scheme of such system resembles a typical smart antenna array block diagram, including the beamforming and direction finding function block.

The coarray concept can be added to this general smart antenna system scheme using the following strategy. First, the array element placement can be physically rearranged, going from a smaller ULA to a sparse array, according to the element spacing of the targeted array. The rest of the analog part in the system stays unaltered. Second, the coarray algorithm is plugged into the system's DoA estimation functional block as a preprocessing block. Before feeding the array signals to the original DoA estimation, this additional block extends the sparsely distributed NULA to a new full virtual ULA (the coarray), which contains more elements than the original NULA and thus corresponds to more inputs. The DoA estimation block uses the coarray input for direction finding. However, it has to be emphasized that the coarray extension is based on the covariance matrix of the input array signals. It does not reconstruct all signals for all virtual array elements. Therefore, the output of the extension may only be used for direction finding. The beamforming block still has to take inputs from the array front end.

For small bandwidths, the necessary time delays for the array elements under beamforming conditions can be

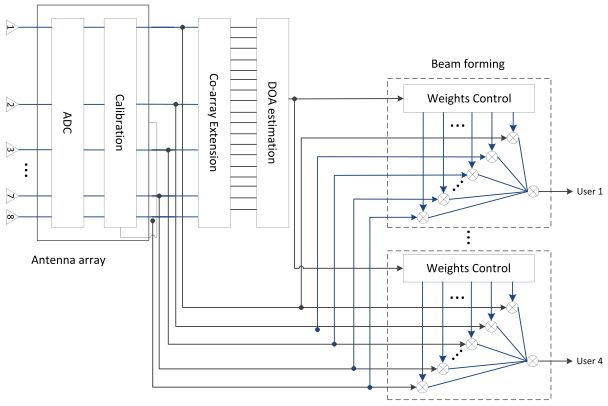

Fig. 5. Implementing a coarray algorithm within MUBTS.

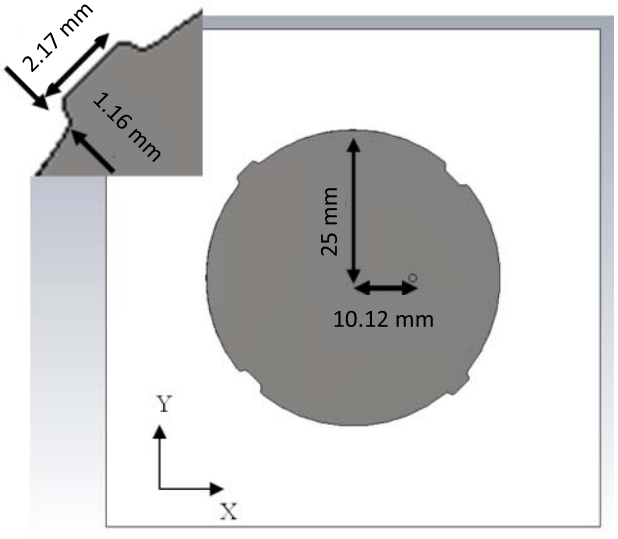

Fig. 6. Topology and dimensions of the antenna element. (The size of the chamfer in the topology is 0.7 mm).

approximated by phase shifting. In the digital domain, a phase shifter can be easily implemented. Depending on the application, either simple delay-and-sum beamforming (match filter) or interference rejection beamforming can be applied to the system by using different weight generation algorithms. The global new smart antenna scheme is shown in Fig. 5. Note that although beamforming using the coarray concept has also been investigated already (see [12], [30], [31]) in this paper, only the DoA estimation block is experimentally studied.

In MUBTS, patch antennas with a working frequency of 1.8 GHz and a bandwidth of 40 MHz are used. Circular polarization is used in order to increase the robustness. More in detail, the antenna element type used is a single-layered probe-fed circular patch topology with four perturbation segments (two indents and two bumps) at its perimeter in order to reach the circular polarization [37]. The use of this type of perturbation is classical in circularly polarized antennas. RO4003 is used as the substrate layer. The topology and dimensions of the radiating patch are shown in Fig. 6. The reflection coefficient of the element is shown in Fig. 7. Based on measurements,

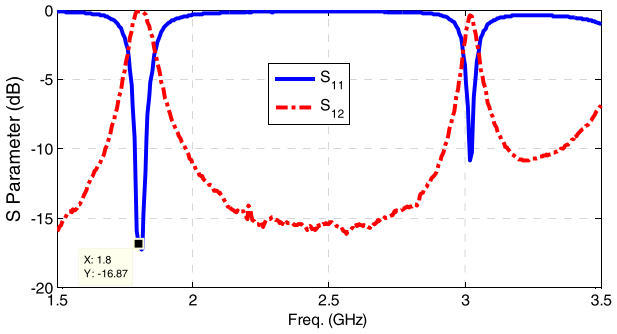

Fig. 7. Measured reflection coefficient of the antenna element (see [37]).

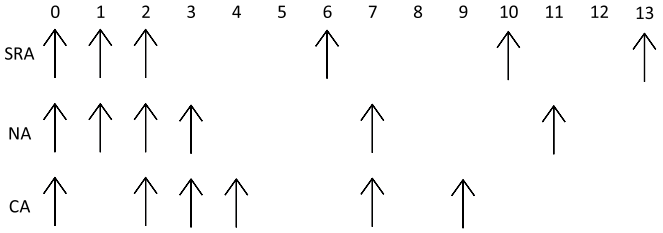

Fig. 8. Geometries of coarrays: NA($P = Q = 3$), SRA [0, 1, 2, 6, 10, 13], and CA ($U = 2$, $V = 3$).

the axial ratio of this element is lower than 3 dB at the operating frequency and in the range from $-50°$ to $50°$.

B. Simulation Results

Although the study reported here focuses on measurements, simulations can be used to set the baseline, i.e., measurements can be compared to simulations performed in an ideal environment without multipath, mutual coupling, and in far-field conditions. This allows to assess the effect of the real environment. In all the numerical analyses performed in the simulation tests, the input source signals are generated by normally distributed pseudorandom functions.

The first comparison is for the arrays with six physical elements: NA ($P = Q = 3$), SRA [0, 1, 2, 6, 10, 13], and CA ($U = 2$, $V = 3$). After applying spatial smoothing, they deliver virtual coarray lengths of $13d$, $11d$, and $9d$, respectively. An ULA ($13d$) is applied here to verify the DoA estimation results. The coarray structures can be seen in Fig. 8. SNR is selected as 10 dB. The results are shown in Fig. 9. The direct result of applying the MUSIC algorithm on a 14-element ($13d$) full ULA under the same circumstances is also shown as a reference. The incident waves coming from six directions are uniformly distributed from $-50°$ to $50°$ with $20°$ of separation.

From Fig. 9, we can clearly see that all three coarrays are able to detect all six sources. Comparing the three coarrays, SRA and NA have a better overall performance over CA. The NA and SRA peaks are visibly sharper and narrower. The accuracy of CA is the worst. Unlike NA and SRA, the CA has a coarray with missing elements and the spatial smoothing-based coarray processing cannot use the entire coarray for the DoA estimation [27].

These coarrays are compared under stricter conditions for an array of five physical elements, which is also used in

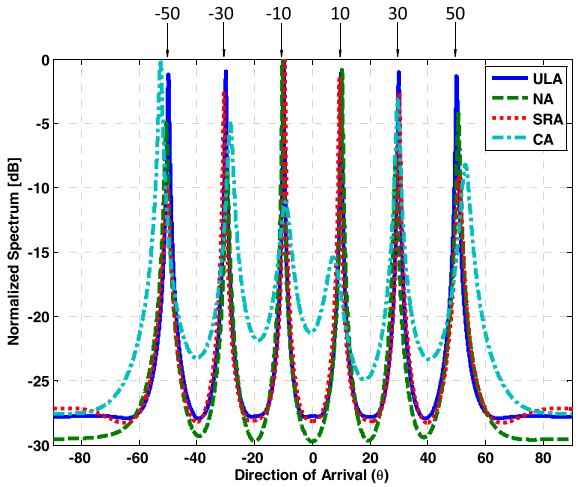

Fig. 9. Typical MUSIC spectra of full length ULA, NA, SRA, and CA for six array elements and six sources. SNR = 10 dB. Number of snapshots = 64.

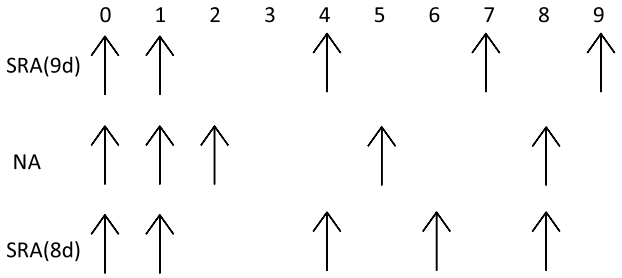

Fig. 10. Geometries of coarrays: NA($P = 2$, $Q = 3$), SRAs $9d$ [0, 1, 4, 7, 9] and $8d$ [0, 1, 4, 6, 8].

the measurements. Under these conditions, the only possible choice for CA ($U = 1$, $V = 4$) is not able to detect more sources than the number of elements. In the simulation, two SRA configurations are chosen: [0, 1, 4, 6, 8] ($8d$) and [0, 1, 4, 7, 9] ($9d$). In order to verify the performance, here we use the ULA ($9d$) as comparison. The coarray structures can be seen in Fig. 10. The SNR stays at 10 dB and the number of snapshots is set to 1600. The angular distribution (in degrees) of the seven sources is $[-52, -37, -23, -6, 13, 28, 43]$, which is exactly the same as chosen in the measurements in the anechoic chamber. The results are shown in Fig. 11.

From Fig. 11, we see that all three coarrays are able to detect all seven sources. Comparing the three coarrays, SRA ($9d$) and NA have a better overall performance over SRA ($8d$), which means that the DoA estimation performance of the SRA has a positive relation to the length of the virtual array.

For further error analysis, the root mean squared error (RMSE) between the detected angles and the real angles for the number of snapshots, ranging from 64 to 2240, was statistically investigated. The simulations were repeated 100 times for each specific case (type of coarray, number of physical elements, and number and direction of sources). The 100 simulations involved 100 different random signals generated by each source. The results are shown in Fig. 12. It is clear to see that the DoA estimation accuracies increase with an increasing number of snapshots. The SRA ($9d$) has

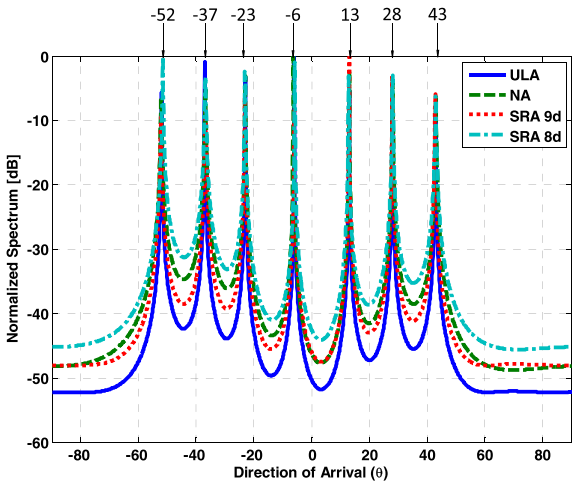

Fig. 11. Typical MUSIC spectra of ULA, NA ($P = 2$, $Q = 3$), and SRAs $9d$ [0, 1, 4, 7, 9] and $8d$ [0, 1, 4, 6, 8] for five array elements and seven sources. SNR = 10 dB. Number of snapshots = 1600.

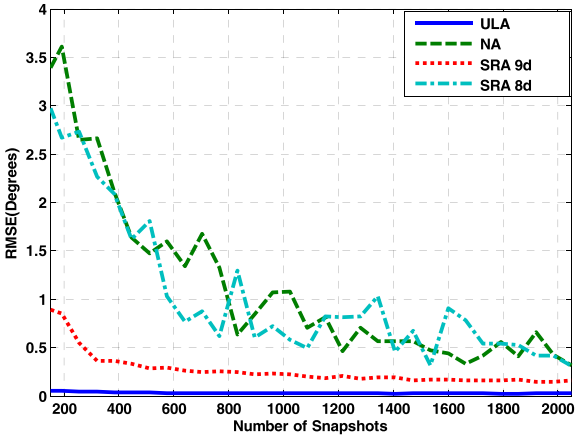

Fig. 12. RMSE in terms of number of snapshots for the full ULA (10 physical elements), NA ($P = 2$, $Q = 3$), and SRAs $9d$ [0, 1, 4, 7, 9] and $8d$ [0, 1, 4, 6, 8] for five array elements and seven sources. SNR = 10 dB.

the best performance among the coarrays. The NA and SRA ($8d$) have similar performances. Also, the fact that the curve does converge to a positive value and not to zero is clearly seen. From the RMSE results, it is also clear to see the nonmonotonicity in all the four arrays. This nonmonotonicity is caused by the difference of the randomly generated signal in each simulation.

C. Measurements Results

In this section, the measurements on the MUBTS platform are discussed. In a real system, the performance may be degraded due to several effects, such as calibration errors, quantization errors, mutual coupling, and circuit imbalances. These effects occur simultaneously. Their incorporation results in a much more realistic study of the performance. This is needed before any practical deployment of a system.

The measurements incorporated redistributions of the physical elements in space, in order to construct different physical arrays.

Fig. 13. Photo of anechoic chamber at ESAT, KU Leuven.

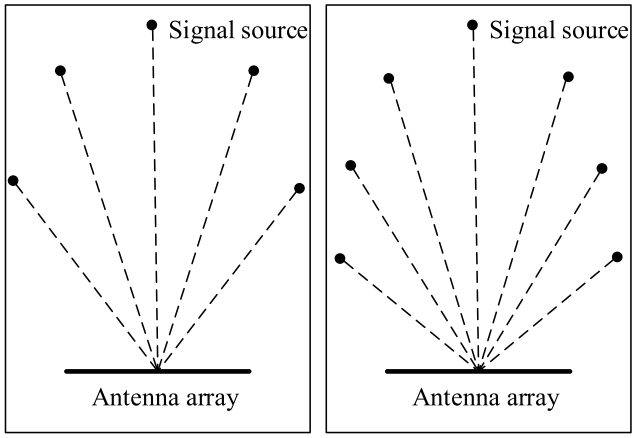

Fig. 14. Distribution of sources in anechoic chamber. Left: five sources. Right: seven sources).

TABLE II

DETECTED ANGLES (IN DEGREES) OF ULA, SRA, NA, AND CA FOR FIVE SOURCES DOA. THE SRA HAS ELEMENTS AT [0, 1, 4, 7, 9], THE NA USES $P = 2$ AND $Q = 3$, AND THE CA USES $U = 2$ AND $V = 3$. THE NUMBER OF SNAPSHOTS IS 640

Actual angle	-30	-10	4	16	32
ULA	-30	-10	3.8	16	31
NA	-31	-9	3.4	17	30
SRA	-30	-9	3.6	15.5	31
CA	×	×	3.5	×	27

Measurements were done both indoors, in an anechoic room, and outdoors, in open air. The length of the full ULA verifying the DoA estimation results is $9d$ (10 physical elements) in all measurements.

1) Anechoic Chamber Measurements: First, measurements were done in an anechoic chamber in order to avoid multipath. Figs. 13 and 14 show the anechoic chamber and the distribution of the transmitters, respectively. The SRA has elements at [0, 1, 4, 7, 9] and length $9d$; the NA uses $P = 2$ and $Q = 3$, and the CA uses $U = 2$ and $V = 3$. The number of snapshots was 640 for five sources and 1600 for seven sources. The results are presented in Fig. 15 and Table II for five sources, and in Fig. 16 and Table III for seven sources, respectively.

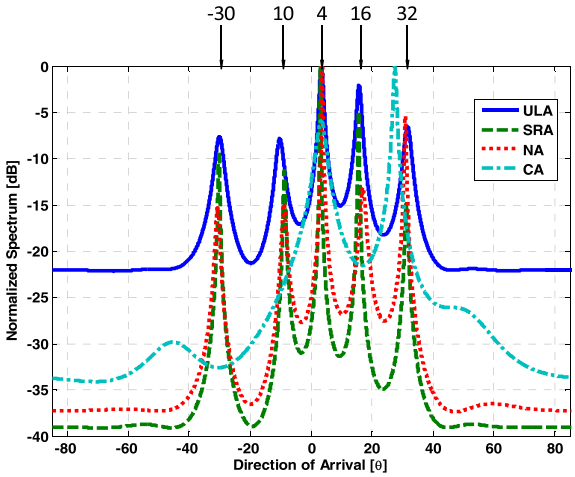

Fig. 15. Typical results from a practical measurement in an anechoic chamber for the detection of five sources with the full ULA and the three coarrays. The SRA has elements at [0, 1, 4, 7, 9] and length $9d$, the NA uses $P = 2$ and $Q = 3$, and the CA uses $U = 2$ and $V = 3$. The number of snapshots was 640.

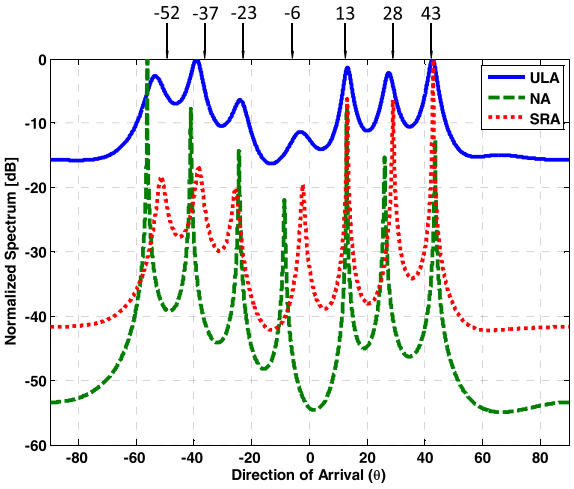

Fig. 16. Typical results from a practical measurement in an anechoic chamber for the detection of seven sources with the full ULA and the two coarrays. The number of snapshots is 1600.

Portable transmitters are used as signal sources. Each transmitter consists of a Spartan 3E FPGA board, a digital to analog converter, and a low-pass reconstruction filter, feeding the baseband-modulated signal to the RF with an in-phase/quadrature (I/Q) modulator. A local oscillator drives the RF input of the modulator with a frequency near 1.8 GHz. All transmitters work with a different frequency offset. Details can be found in [37]. All sources were set for certain distances (larger than 10λ with $\lambda = 0.17$ m to assure far-field conditions) and output signal strengthens to make sure that the SNR after reception in all the array elements was in the range 10–15 dB (compared to the noise floor). The type of source is an in-house designed portable transmitter. More details can be found in [37].

The result in Fig. 15 shows that even with 640 snapshots or more, the CA is not able to detect all DoAs. The other two coarrays (SRA and NA) perform much better. This confirms

TABLE III

DETECTED ANGLES (IN DEGREES) OF ULA, SRA, AND NA FOR SEVEN SOURCES DoA. THE SRA HAS ELEMENTS AT [0, 1, 4, 7, 9], THE NA USES $U = 2$ AND $V = 3$. THE NUMBER OF SNAPSHOTS IS 1600

Actual angle	-52	-37	-23	-6	13	28	43
ULA	-53	-39	-24	-3	13	28	43
NA	-57	-41	-25	-9	13	26	44
SRA	-51	-38	-26	-3	13	29	43

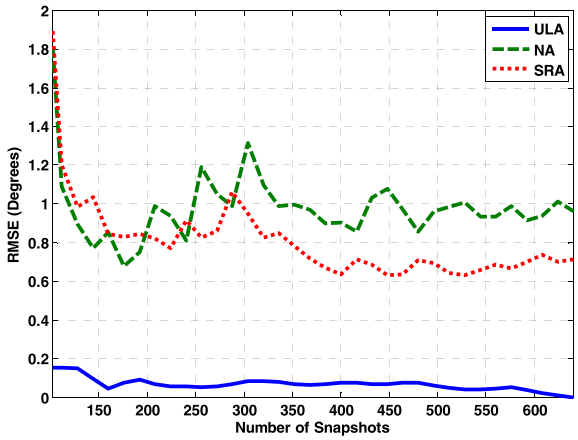

Fig. 17. RMSE as a function of the number of snapshots for five sources. The reference level is the DoA for 640 snapshots.

to the theoretical and the simulation results available in the literature. Even with one more element, the CA is not able to detect all sources due to the missing elements in the coarray, which invokes a much lower degree of freedom. The errors in the results of SRA and NA are acceptable, given the nonideal conditions of the experimental setup.

In Fig. 16 and Table III, only the SRA and NA are given because of the fact that the number of sources, i.e., seven, exceeds the maximal number of sources that can be identified by a $U = 2$, $V = 3$ CA algorithm. For seven sources, the number of snapshots goes up to 1600 in order to get an acceptable result.

It is clearly seen that based on real measurements on a state-of-the-art platform, the results deteriorate. Due to the smearing of the peaks, erroneous results can be obtained. However, it is also clearly demonstrated that the SRA can detect all sources.

In order to quantitatively show how the coarray algorithms are converging, an analysis of the accuracy which refers to the RMSE between the measured results and the actual source locations for all sources in terms of the number of snapshots is shown in Figs. 17 and 18. It is easy to see the general trend that the accuracies of both the NA and the SRA increase with an increasing number of snapshots. All the indoor RMSE results are calculated as the average of five consecutive measurements. Due to the signal variation and lack of repetition, nonsmoothness and nonmonotonicity, which can be also found in the simulated RMSE results, are observed in the results. Comparing the results with the simulation results, the RMSE values of the indoor measurements are similar to the simulation results and within an acceptable range, which is smaller than 2°.

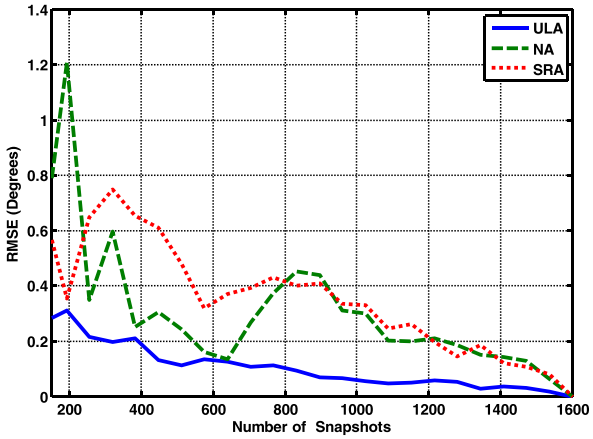

Fig. 18. RMSE as a function of the number of snapshots for seven sources. The reference level is the DoA for 1600 snapshots.

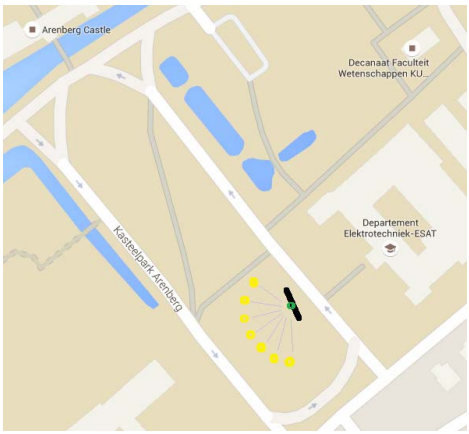

Fig. 19. Green dot: location of the receiving array. Black line: alignment of the antenna elements. Yellow dots: locations of the sources.

TABLE IV

DETECTED ANGLES (IN DEGREES) OF ULA, SRA, NA FOR FIVE SOURCES DoA IN FIG. 20. THE SRA HAS ELEMENTS AT [0, 1, 4, 7, 9], THE NA USES $P = 2$ AND $Q = 3$, THE CA USES $U = 2$ AND $V = 3$. THE NUMBER OF SNAPSHOTS IS 1600

Actual angle(aligned)	-51	-27	-5	19	44
ULA	-52.61	-25.42	-4.34	21.5	43.02
NA	-51.26	-24.09	-7.08	21.87	52.83
SRA	-57.31	-25.58	-4.62	20.56	43.36

2) Outdoor Measurements: Measurements were also performed outdoors in open air in order to investigate the performance of the coarray algorithms in a more practical situation. In order to minimize the effects of the multipath phenomenon, the location was chosen in an open grass land, which is the meadow in front of the Arenberg Castle, Leuven (see Fig. 19).

The three coarrays were configured in the same way as for the measurements in the anechoic chamber. The results for five sources are shown in Fig. 20 and Table IV, and for six sources in Fig. 21 and Table V, respectively.

The results clearly show that with five sources and 1600 snapshots, both NA and SRA are able to detect

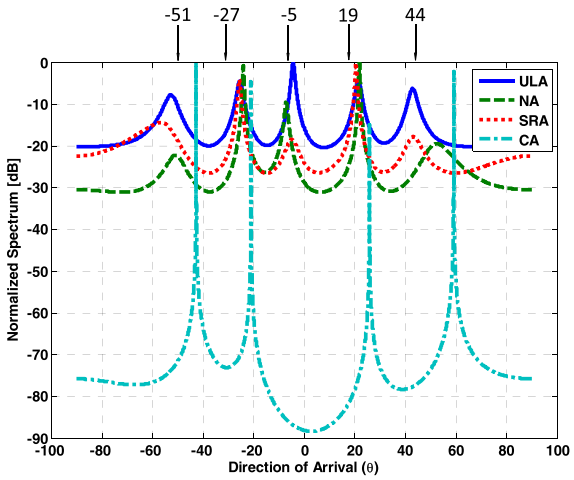

Fig. 20. Measurement results for the three coarrays and the full 10-element ULA for five sources. Only the SRA and the NA deliver useful DoAs. The number of snapshots is 1600.

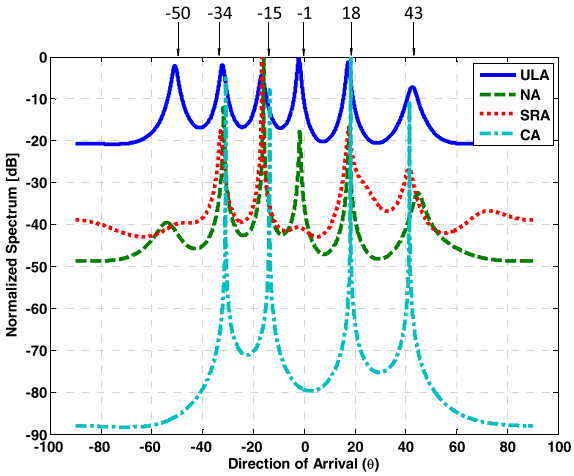

Fig. 21. Measurement results for the three coarrays and the full 10-element ULA for six sources. Only the SRA and the NA deliver useful DoAs. The number of snapshots is 1600.

TABLE V

DETECTED ANGLES (IN DEGREES) OF ULA, SRA, NA FOR SIX SOURCES DOA IN FIG. 21. THE SRA HAS ELEMENTS AT [0, 1, 4, 7, 9], THE NA USES $P = 2$, $Q = 3$. THE NUMBER OF SNAPSHOTS IS 1600

Actual angle(aligned)	-50	-34	-15	-1	18	43
ULA	-51	-32.31	-16.73	-2.17	17.2	42.54
NA	-54.49	-31.98	-16.12	-1.63	17.47	44.82
SRA	-47.42	-33.05	-16.8	-2	17.49	41.3

all sources. Compared with the results in the anechoic chamber, the resolution and accuracy decrease. This is caused by the multipath components in the outdoor environment. When the number of sources increases to six, although all the sources can be detected, some peaks are almost indistinguishable even with a large number of snapshots.

An error analysis of the RMSE between the detected angles and the actual angles in terms of the number of snapshots of these measurements is shown in Figs. 22 and 23. All the outdoor RMSE are also calculated as the average

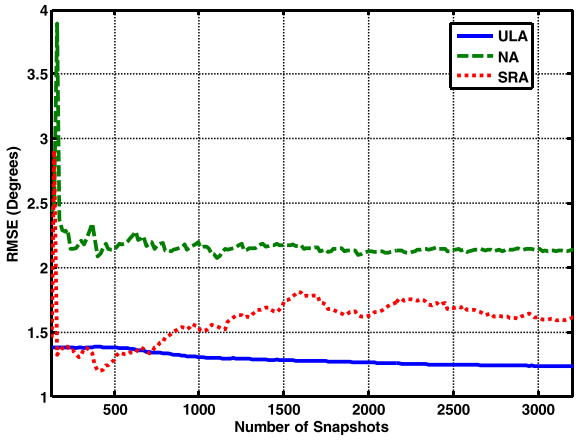

Fig. 22. RMSE using the actual angles as a reference, for five sources.

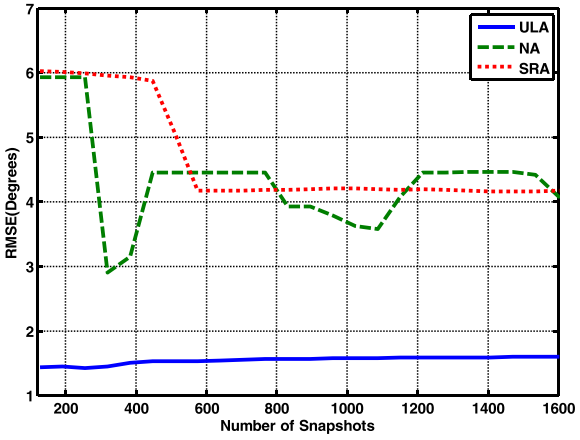

Fig. 23. RMSE using the actual angle as a reference, for six sources.

of five consecutive measurements. Because of the fact that the coprime array fails to deliver high-quality DoA results, it was not considered in these figures. Also, if a coarray failed to deliver a result for a certain source below a certain snapshot size, the error is counted as half the distance to the next source location (approx. 8°–10°).

It is clearly seen that the SRA DOA estimation is slightly more reliable in comparison with the NA. CA is inferior with respect to these two. Compared with NA and SRA, the coarray generated by CA is not a full ULA but it misses elements, which degrades the degree of freedom and the performance significantly [27].

This experimentally confirms the conclusion from the simulation results: for the same array length, the SRA has a slightly superior performance over the CA and NA. Note that a "steady-state error" is visible in the results. Namely, after a certain snapshot length, the output of the coarray algorithms is no longer converging to the full ULA MUSIC results. This error could be caused by mutual coupling between the antenna elements, next to other problems such as imperfect calibrations (not fulfilling the far-field condition during calibration) or the multipath phenomenon. As we can see from all the RMSE results, the RMSE converges to a positive value instead of zero. In (ideal) simulations, all antenna elements are consid-

ered to be receiving signals independently of each other. From the results, it is clear that the error of the indoor measurement is much smaller than the error of the outdoor measurement due to the reduction of the multipath phenomenon.

Since the average distance between the antenna elements in a sparse array is larger than the distance between the elements in an ULA, the effect of the mutual coupling should be less severe. A general discussion of the effect of mutual coupling on sparse arrays can be found in [43]. However, in contrast to a "physical" ULA, where all the elements are physically present, in a coarray, the elements of the virtual ULA are "constructed" from a limited number of elements physically present. Therefore, the distortions of the signal from the physical elements systematically affect the related virtual elements, which have a computational relation (through the spatial smoothing process) with this element. Actually, every phenomenon generating a difference between the real signal received by a physical element and the theoretical signal assumed at that element is subject to this scenario: not only mutual coupling but also calibration error, circuit noise, multipath effect, and so on. This systematic error propagation leads to an asymptotic error in the measurement results [44], which is a common effect in many unwrapping phase-based methods. Obviously in an ULA, the calibration error and circuit noise are, in general, independent for each element and mutual coupling mostly affects only the nearby elements without propagating much further. Averaging the received signals from an ULA reduces the total system error, as also described for array geometry perturbation in [45].

Comparing the measurement results in the anechoic chamber with the outdoor results, it is clear to see that the results in the anechoic chamber are much better than the outdoor results, especially for the coarrays. The RMSEs of the ULA for both indoor and outdoor measurements are in the acceptable range. However, the performances of the coarrays differ a lot. The RMSEs of the measurements in anechoic chamber are always within 2° and the RMSEs of the outdoor measurements are much larger, even up to 7°. The only difference between these two measurements is that uncontrollable multipath signals are present in the outdoor measurements. This could mean that the MUSIC-based coarray DoA estimation algorithms lack the ability to compensate for the effect of multipath phenomena. Based on both the simulation results and the measurement results, it can be concluded that MUSIC combined with spatial smoothing is not suitable for coarrays such as SRA, NA, and CA to estimate DoAs in state-of-the-art practical systems based on low-cost commercial off-the-shelf components. Improved methods for better performance are proposed in [22]–[31].

Also, the coarray concept may suffer from a higher amount of saturation (caused by the limited voltage range of the analog-to-digital converter, PA, and so on), in comparison to the full ULA for the same reason.

IV. Conclusion

Three recently developed compressive sensing coarray algorithms exploiting the Khatri–Rao product concept to synthesize a larger coarray were implemented on Katholieke Universiteit Leuven's recently developed MUBTS system: the SRA, NA, and CA. The performance is compared through both simulations and real measurements. The relationship between the DoA accuracy and the number of snapshots is also investigated. From the results, it is clear that among these three coarrays, the SRA has a better performance, both in simulations and in real measurements. However, comparing the measurement results with the simulation results, it can be concluded that MUSIC combined with spatial smoothing is not suitable for coarrays such as SRA, NA, and CA to estimate DoAs in practical applications with the presence of multipath signals. This conclusion contrasts the results as obtained in [5] and [6], where the effect of multipath on DoA estimation is mitigated by using spatial smoothing for conventional DoA estimation algorithms. It is a very strong conclusion which could be of prime concern for manufacturers of 5G antenna systems.

References

[1] S. U. Pillai, Y. Bar-Ness, and F. Haber, "A new approach to array geometry for improved spatial spectrum estimation," *Proc. IEEE*, vol. 73, no. 10, pp. 1522–1524, Oct. 1985.

[2] Y. I. Abramovich, D. A. Gray, A. Y. Gorokhov, and N. K. Spencer, "Positive-definite Toeplitz completion in DOA estimation for nonuniform linear antenna arrays. I. Fully augmentable arrays," *IEEE Trans. Signal Process.*, vol. 46, no. 9, pp. 2458–2471, Sep. 1998.

[3] Y. Abramovich, N. K. Spencer, and A. Y. Gorokhov, "Positive-definite Toeplitz completion in DOA estimation for nonuniform linear antenna arrays. II. Partially augmentable arrays," *IEEE Trans. Signal Process.*, vol. 47, no. 6, pp. 1502–1521, Jun. 1999.

[4] R. O. Schmidt, "Multiple emitter location and signal parameter estimation," *IEEE Trans. Antennas Propag.*, vol. AP-34, no. 3, pp. 276–280, Mar. 1986.

[5] Y. Yang, C. Wan, C. Sun, and Q. Wang, "DOA estimation for coherent sources in beamspace using spatial smoothing," in *Proc. Joint Conf. 4th Int. Conf. Inf., Commun. Signal Process. 4th Pacific Rim Conf. Multimedia*, vol. 2. Dec. 2003, pp. 1028–1032.

[6] B. D. Rao and K. V. S. Hari, "Effect of spatial smoothing on the performance of MUSIC and the minimum-norm method," *IEE Proc. F Radar Signal Process.*, vol. 137, no. 6, pp. 449–458, Dec. 1990.

[7] Q. Yuan, Q. Chen, and K. Sawaya, "Accurate DOA estimation using array antenna with arbitrary geometry," *IEEE Trans. Antennas Propag.*, vol. 53, no. 4, pp. 1352–1357, Apr. 2005.

[8] Q. Yuan, Q. Chen, and K. Sawaya, "Experimental study on MUSIC-based DOA estimation by using universal steering vector," *IEICE Trans. Commun.*, vol. E91-B, no. 5, pp. 1575–1580, May 2008.

[9] R. T. Hoctor and S. A. Kassam, "The unifying role of the coarray in aperture synthesis for coherent and incoherent imaging," *Proc. IEEE*, vol. 78, no. 4, pp. 735–752, Apr. 1990.

[10] R. J. Kozick and S. A. Kassam, "Coarray synthesis with circular and elliptical boundary arrays," *IEEE Trans. Image Process.*, vol. 1, no. 3, pp. 391–405, Jul. 1992.

[11] A. Moffet, "Minimum-redundancy linear arrays," *IEEE Trans. Antennas Propag.*, vol. AP-16, no. 2, pp. 172–175, Mar. 1968.

[12] P. Pal and P. P. Vaidyanathan, "Nested arrays: A novel approach to array processing with enhanced degrees of freedom," *IEEE Trans. Signal Process.*, vol. 58, no. 8, pp. 4167–4181, Aug. 2010.

[13] A. Massa, P. Rocca, and G. Oliveri, "Compressive sensing in electromagnetics—A review," *IEEE Antennas Propag. Mag.*, vol. 57, no. 1, pp. 224–238, Feb. 2015.

[14] P. Rocca, G. Oliveri, R. J. Mailloux, and A. Massa, "Unconventional phased array architectures and design methodologies—A review," *Proc. IEEE*, vol. 104, no. 3, pp. 544–560, Mar. 2016.

[15] D. D. Ariananda and G. Leus, "Direction of arrival estimation for more correlated sources than active sensors," *Signal Process.*, vol. 93, no. 12, pp. 3435–3448, Dec. 2013.

[16] I. Bilik, "Spatial compressive sensing for direction-of-arrival estimation of multiple sources using dynamic sensor arrays," *IEEE Trans. Aerosp. Electron. Syst.*, vol. 47, no. 3, pp. 1754–1769, Jul. 2011.

[17] W.-K. Ma, T.-H. Hsieh, and C.-Y. Chi, "DOA estimation of quasi-stationary signals via Khatri–Rao subspace," in *Proc. IEEE Int. Conf. Acoust., Speech Signal Process. (ICASSP)*, Apr. 2009, pp. 2165–2168.

[18] S. Shakeri, D. D. Ariananda, and G. Leus, "Direction of arrival estimation using sparse ruler array design," in *Proc. 13th Int. Workshop Signal Process. Adv. Wireless Commun. (SPAWC)*, Jun. 2012, pp. 525–529.

[19] P. Pal and P. P. Vaidyanathan, "Coprime sampling and the MUSIC algorithm," in *Proc. Digit. Signal Process. Workshop IEEE Signal Process. Edu. Workshop (DSP/SPE)*, Jan. 2011, pp. 289–294.

[20] G. Oliveri and A. Massa, "Compressive sensing in electromagnetics: Theoretical foundations, recent advances, and applicative guidelines," in *Proc. Eur. Conf. Antennas Propag. (EuCAP)*, Apr. 2014, pp. 1243–1246.

[21] M. Wang and A. Nehorai, "Coarrays, MUSIC, and the Cramér–Rao bound," *IEEE Trans. Signal Process.*, vol. 65, no. 4, pp. 933–946, Feb. 2017.

[22] K. Han, P. Yang, and A. Nehorai, "Calibrating nested sensor arrays with model errors," *IEEE Trans. Antennas Propag.*, vol. 66, no. 11, pp. 4739–4748, Nov. 2015.

[23] Y. Iizuka and K. Ichige, "Extension of two-level nested array with larger aperture and more degrees of freedom," in *Proc. Int. Symp. Antennas Propag. (ISAP)*, Oct. 2016, pp. 442–443.

[24] C.-L. Liu and P. P. Vaidyanathan, "Super nested arrays: Linear sparse arrays with reduced mutual coupling—Part I: Fundamentals," *IEEE Trans. Signal Process.*, vol. 64, no. 15, pp. 3997–4012, Aug. 2016.

[25] C.-L. Liu and P. P. Vaidyanathan, "Super nested arrays: Linear sparse arrays with reduced mutual coupling—Part II: High-order extensions," *IEEE Trans. Signal Process.*, vol. 64, no. 16, pp. 4203–4217, Aug. 2016.

[26] M. Yang, L. Sun, X. Yuan, and B. Chen, "Improved nested array with hole-free DCA and more degrees of freedom," *Electron. Lett.*, vol. 52, no. 25, pp. 2068–2070, Dec. 2016.

[27] P. P. Vaidyanathan and P. Pal, "Sparse sensing with co-prime samplers and arrays," *IEEE Trans. Signal Process.*, vol. 59, no. 2, pp. 573–586, Feb. 2011.

[28] C.-L. Liu, P. P. Vaidyanathan, and P. Pal, "Coprime coarray interpolation for DOA estimation via nuclear norm minimization," in *Proc. IEEE Int. Symp. Circuit Syst. (ISCAS)*, May 2016, pp. 2639–2642.

[29] J. Ramirez and J. Krolik, "Multiple source localization with moving co-prime arrays," in *Proc. IEEE Int. Conf. Acoust., Speech Signal Process. (ICASSP)*, Apr. 2015, pp. 2374–2378.

[30] K. Adhikari, J. R. Buck, and K. E. Wage, "Beamforming with extended co-prime sensor arrays," in *Proc. IEEE Int. Conf. Acoust., Speech Signal Process. (ICASSP)*, Vancouver, BC, Canada, May 2013, pp. 4183–4186.

[31] P. Pal and P. P. Vaidyanathan, "Beamforming using passive nested arrays of sensors," in *Proc. IEEE Int. Symp. Circuits Syst.*, Paris, France, May/Jun. 2010, pp. 2840–2843.

[32] N. Xiang, D. Bush, and J. E. Summers, "Experimental validation of a coprime linear microphone array for high-resolution direction-of-arrival measurements," *J. Acoust. Soc. Amer.*, vol. 134, no. 4, p. EL261, Apr. 2015.

[33] Q. Shen, W. Liu, W. Cui, S. Wu, Y. D. Zhang, and M. G. Amin, "Low-complexity direction-of-arrival estimation based on wideband co-prime arrays," *IEEE/ACM Trans. Audio, Speech, Language Process.*, vol. 23, no. 9, pp. 1445–1456, Sep. 2015.

[34] S. A. Alawsh, M. T. Alkhodary, A. H. Muqaibel, and M. S. Sharawi, "Experimental evaluation of coprime sampler in direction of arrival estimation," in *Proc. IEEE Middle East Conf. Antennas Propag. (MECAP)*, Sep. 2016, pp. 1–4.

[35] K. Morokuma, A. Takemoto, and Y. Karasawa, "A novel high-resolution propagation measurement scheme for indoor terrestrial TV signal reception based on two-dimensional virtual array technique," *IEICE Trans. Commun.*, vol. E96-B, no. 4, pp. 986–993, Apr. 2013.

[36] S. Kang, S. Lee, J.-E. Lee, and S.-C. Kim, "Improving the performance of DOA estimation using virtual antenna in automotive radar," *IEICE Trans. Commun.*, vol. E100-B, no. 5, pp. 771–778, May 2017.

[37] H. Xu, H. Aliakbarian, E. Van der Westhuizen, R. Wolhuter, and G. A. E. Vandenbosch, "An architectural scheme for real-time multiple users beam tracking systems," *IEEE Syst. J.*, vol. 11, no. 4, pp. 2905–2916, Dec. 2017.

[38] J. Leech, "On the Representation of 1, 2, …, *n* by differences," *J. London Math. Soc.*, vol. 31, pp. 160–169, Apr. 1956.

[39] J. E. Evans, "High resolution angular spectrum estimation technique for terrain scattering analysis and angle of arrival estimation," in *Proc. 1st ASSP Workshop Spectral Estimation*, Hamilton, ON, Canada, Aug. 1981, pp. 134–139.

[40] T.-J. Shan, M. Wax, and T. Kailath, "On spatial smoothing for direction-of-arrival estimation of coherent signals," *IEEE Trans. Acoust., Speech, Signal Process.*, vol. ASSP-33, no. 4, pp. 806–811, Apr. 1985.

[41] J. Yan, Y. Huang, H. Xu, and G. A. E Vandenbosch, "Hardware acceleration of MUSIC based DoA estimator in MUBTS," in *Proc. Eur. Conf. Antennas Propag. (EuCAP)*, Apr. 2014, pp. 2561–2565.

[42] H. Xu, H. Aliakbarian, and G. A. E. Vandenbosch, "Off-the-shelf low-cost target tracking architecture for wireless communications," *IEEE Syst. J.*, vol. 9, no. 1, pp. 13–21, Mar. 2015.

[43] E. BouDaher, F. Ahmad, M. G. Amin, and A. Hoorfar, "Effect of mutual coupling on direction-of-arrival estimation using sparse dipole arrays," in *Proc. IEEE Int. Symp. Antennas Propag. (APSURSI)*, Jun./Jul. 2016, pp. 2189–2190.

[44] Z. Weng and P. Djuric, "A search-free DOA estimation algorithm for coprime arrays," *Digit. Signal Process.*, vol. 24, pp. 27–33, Jan. 2014.

[45] A. Koochakzadeh and P. Pal, "Sparse source localization in presence of co-array perturbations," in *Proc. Int. Conf. Sampling Theory Appl. (SampTA)*, Washington, DC, USA, 2015, pp. 563–567.

Jiachen Wang (S'17) was born in Jiangxi, China, in 1990. He received the bachelor's degree in electronic and information engineering from Zhejiang University, Hangzhou, Zhejiang, China, in 2011, and the M.S. degree in electrical engineering from Katholieke Universiteit Leuven, Leuven, Belgium, in 2014, where he is currently pursuing the Ph.D. degree with the TELEMIC Research Division, Electrical Engineering Department.

His current research interests include DoA estimation algorithms, beam steering technology, and array signal processing.

Hantao Xu (S'12) was born in Guangzhou, Guangdong, China. He received the bachelor's degree in electronics and information engineering from South China Agricultural University, Guangdong, in 2008, the M.S. degrees (*cum laude*) in electronics engineering and electrical engineering from the GroepT Hoge School, Katholieke Universiteit Leuven, Leuven, Belgium, in 2009 and 2011, respectively, and the Ph.D. degree from the ESAT-TELEMIC Research Division, Katholieke Universiteit Leuven, in 2016, under supervision of Prof. G. A. E. Vandenbosch.

He is currently an ASIC/FPGA Design and Validation Engineer with Nokia Bell NV, Antwerpen, Belgium. His current research interests include optical links to mobile front haul design and signal processing architecture for telecommunication.

Geert J. T. Leus (M'01–SM'05–F'13) received the M.Sc. and Ph.D. degrees in electrical engineering from Katholieke Universiteit Leuven, Leuven, Belgium, in 1996 and 2000, respectively.

He is currently an Antoni Van Leeuwenhoek Full Professor with the Faculty of Electrical Engineering, Mathematics, and Computer Science, Delft University of Technology, Delft, The Netherlands. His current research interests include the broad area of signal processing, with a specific focus on wireless communications, array processing, sensor networks, and graph signal processing.

Dr. Leus was a member at large of the Board of Governors of the IEEE Signal Processing Society, the Chair of the IEEE Signal Processing for Communications and Networking Technical Committee, a member of the IEEE Sensor Array and Multichannel Technical Committee, and the Editor-in-Chief of the *EURASIP Journal on Advances in Signal Processing*. He is a Fellow of EURASIP. He was a recipient of the 2002 IEEE Signal Processing Society Young Author Best Paper Award and the 2005 IEEE Signal Processing Society Best Paper Award. He was on the Editorial Boards of the IEEE TRANSACTIONS ON SIGNAL PROCESSING, the IEEE TRANSACTIONS ON WIRELESS COMMUNICATIONS, IEEE SIGNAL PROCESSING LETTERS, and the *EURASIP Journal on Advances in Signal Processing*. He is currently the Vice-Chair of the EURASIP Special Area Team on Signal Processing for Multisensor Systems, an Associate Editor of Foundations and Trends in Signal Processing, and the Editor-in-Chief of EURASIP Signal Processing.

Guy A. E. Vandenbosch (M'92–SM'08–F'13) received the M.S. and Ph.D. degrees in electrical engineering from Katholieke Universiteit Leuven (KU Leuven), Leuven, Belgium, in 1985 and 1991, respectively.

In 2014, he was a Visiting Professor with Tsinghua University, Beijing, China. Since 1993, he has been a Lecturer with ESAT, KU Leuven. Since 2005, he has been a Full Professor with KU Leuven. He has taught or teaches courses on electromagnetic waves, antennas, electromagnetic compatibility, fundamentals of communication and information theory, electrical engineering, electronics, and electrical energy, and digital steer- and measuring techniques in physics. He has authored or co-authored in ca. 280 papers in international journals and has led to ca. 370 presentations at international conferences. His current research interests include electromagnetic theory, computational electromagnetics, planar antennas and circuits, nanoelectromagnetics, EM radiation, EMC, and bioelectromagnetics.

Dr. Vandenbosch was the President of SITEL, the Belgian Society of Engineers in Telecommunication and Electronics from 2001 to 2007. From 2008 to 2014, he was a member of the board of FITCE Belgium, the Belgian branch of the Federation of Telecommunications Engineers of the European Union. From 1999 to 2004, he was the Vice-Chairman, a Secretary from 2005 to 2009, and the Chairman of the IEEE Benelux Chapter on Antennas en Propagation from 2010 to 2016. From 2002 to 2004, he was a Secretary of the IEEE Benelux Chapter on EMC. From 2012 to 2014, he was a Secretary of the Belgian National Committee for Radio-electricity, where he is also in charge of commission E.